
A LEVEL SET KALMAN FILTER APPROACH TO ESTIMATE THE CIRCADIAN PHASE AND ITS UNCERTAINTY FROM WEARABLE DATA

Dae Wook Kim^{1,*}, Minki P. Lee^{1,*}, and Daniel B. Forger^{1,2,†}

¹Department of Mathematics, University of Michigan, Ann Arbor, MI

²Department of Computational Medicine and Bioinformatics, University of Michigan, Ann Arbor, MI

July 20, 2022

Abstract

Daily (~ 24 hr) rhythms of behavior and physiology such as sleep and hormone secretion are coordinated by an endogenous timer, the circadian clock. The accurate estimation of the clock state (i.e., the circadian phase) outside of the laboratory has enormous potential for precision medicine. Several methods that predict the phase from measurements collected with wearables (e.g., Apple Watch) have been recently developed. However, computation of the uncertainty in the estimation remains an open problem. The uncertainty analysis is necessary because the estimation accuracy can largely change even by a small perturbation of daily routine. Here, we present a method to account for the uncertainty and estimate the circadian phase using a new extension of Kalman filtering named the level set Kalman filter. Using the newly proposed method, we study the relationship between phase uncertainty and process noise from various sources. This allows the identification of the magnitude of the noise in the circadian system, which is impossible with previous methods. Moreover, our study reveals how much the uncertainty of the phase estimate of the central clock that is inaccessibly located in the brain can be reduced when measurements of the peripheral clock phase are given from wearables. We also show that our method has a performance improvement over the previous methods. Finally, we apply our method to real-world data to further identify its usefulness. These results set the stage for systematically understanding the circadian dynamics in the real world.

Keywords: level set Kalman filter, nonlinear estimation, mathematical models, circadian rhythms, wearable data

1 Introduction

Circadian rhythms are ~ 24 hr oscillations in diverse behavioral and physiological processes observed in nearly all living organisms [11]. In mammals, including humans, the daily rhythms are coordinated with the external light-dark cycles by an innate timing system, the circadian clock [55]. This system has a hierarchical structure where the master pacemaker in the hypothalamic suprachiasmatic nucleus controls clocks in peripheral tissues (e.g., the heart circadian clock) by sending neuronal and hormonal signals [23, 25]. The failure of synchrony between the master clock and the peripheral clocks can occur, for instance, due to an alteration of the external environment. Notably, around 80% of the population appears to live a shift work lifestyle [53]. This increases

This work was funded by Human Frontiers Science Program Organization Grant RGP0019/2018 and NSF DMS grant 2052499. DBF is the CSO of Arcascope, a company that makes circadian rhythms software. Both he and the University of Michigan own equity in Arcascope.

* These authors contributed equally.

† Correspondence: forger@umich.edu

the risk for various chronic diseases, such as sleep disorders, mental illnesses, cancer, and diabetes [53, 63]. Thus, tools to calculate sleep schedules rapidly restoring desynchronization have recently received attention [24, 58]. Targets of more than 80% of currently approved drugs have daily rhythmic activity [45, 62]. As a result, the efficacy and toxicity of diverse drugs, including around 50 anticancer drugs, largely change upon dosing time [33]. Thus, many clinical trials have been performed to develop a pharmaceutical intervention that considers the patient’s circadian phase, so-called chronotherapy [44, 45]. To realize chronotherapy, we need the precise measurement of an individual’s circadian phase in real-world settings.

One of the promising tools for this is wearable technology. Wearable devices already owned by millions of individuals track physiological proxies of clocks, such as rest-activity rhythms, heart rate (HR), skin temperature, and sleep outside of the laboratory [33]. However, because only the downstream signals can be monitored by wearables, suitable follow-up analysis techniques are required to infer the unobservable circadian phase of the central pacemaker located deep in the brain. One approach is to predict the phase using differential equation models of the human circadian clock, coupled with activity or light levels recorded from wearables [26, 52, 61]. Specifically, a van der Pol limit cycle model that takes light or activity measurements as the direct input has been proposed to predict the circadian phase [15, 26]. Another recent approach is to demask noisy measurements of the HR rhythm affected by various confounding factors, such as activity, stress, and hormones, using a Bayesian framework with harmonic-regression-plus-autoregressive-noise models [4, 40]. This allows one to estimate a phase of the peripheral clock, the HR phase, and infer the phase of the master clock based on their experimentally identified relationship. Although these methods clearly show the usefulness of the combined approach of wearable technology and mathematical analysis, they have limitations. Specifically, the uncertainty of the central clock phase cannot be estimated using the previous methods [26, 52, 61]. As a result, the relationship between the circadian phase uncertainty and the process noise in the circadian clock from various sources remains to be elucidated. Moreover, the information available from wearable monitoring is not fully exploited. For instance, the phase of the peripheral clock hidden in HR measurements is not utilized in the previous studies [26, 38, 52, 61, 64]. Thus, further studies are required to check whether the performance of estimating the unobservable master clock state can be improved with indirect information (e.g., the HR phase).

One way to address this is to use a Bayesian filtering approach that updates a state estimation of the target given knowledge of the system and indirect measurements [47]. Specifically, we can formulate the phase estimation problem as a filtering problem with nonlinear continuous-discrete state-space models [1, 48] of the form

$$\begin{aligned} d\mathbf{x}_t &= \mathbf{v}(\mathbf{x}_t, t)dt + \sqrt{\mathbf{K}}dW_t \\ \mathbf{z}_k &= h(\mathbf{x}_{t_k}) + \epsilon_k \end{aligned} \tag{1}$$

where \mathbf{x}_t denotes the n -dimensional state of the central pacemaker at time t whose dynamics is described with a nonlinear drift function \mathbf{v} ; W_t denotes the n -dimensional standard Brownian motion; $\mathbf{K} \in \mathbb{R}^{n \times n}$ is called diffusion matrix; \mathbf{z}_k and h denote the measurement and the measurement function, respectively; and the measurement noise ϵ_k is assumed to be Gaussian with zero mean and known covariance $\mathbb{E}[\epsilon_i \epsilon_j^T] = R_i \delta(i - j)$. The symbol δ denotes the Kronecker delta. Previously, this problem was handled using a sequential Monte Carlo method called a particle filter with core body temperature measurements under laboratory conditions [41]. This shows the potential of the filtering approach on real-world data collected with wearables. However, applying the particle filter [41] to wearable data is challenging. A major complication includes its huge computational cost to analyze high-frequency long-term longitudinal real-world wearable measurements (e.g., > 60 days) compared to the ones from the laboratory (e.g., < 3 days). Moreover, many confounding factors in free-living conditions that affect the peripheral clocks on the hour timescale lead to the temporal-correlated noise structure in wearable data [4]. This makes estimating the peripheral clock phase challenging, which corresponds to the measurement \mathbf{z}_k in our filtering problem, for instance, with the ordinary least squares method [7, 14].

Here, we developed a method to estimate the circadian phase and its uncertainty from wearable data by combining the new extension of Kalman filtering called the level set Kalman filter (LSKF) [59] and the recently developed Bayesian framework [4]. Specifically, by applying the Bayesian framework to activity and HR measurements collected with wearables, the phase estimate of the peripheral clock (i.e., the HR phase) and its uncertainty are obtained. Given the knowledge of the peripheral clock state, we compute the estimate of the master clock phase and its uncertainty using the LSKF [59]. This can account for the uncertainty in the master clock state, which is impossible with the previous methods [26, 52, 61]. Numerical experiments

show that our method has a consistent performance improvement over the previous methods. We also apply the method to real-world data to further demonstrate its usefulness.

The rest of the paper is structured as follows: In section 2, we review previous approaches to estimate the state of the circadian clock and describe the novelty of our approach. In section 3, we define our continuous-discrete filtering problem for estimating the circadian phase and describe our approach to solve the problem. Then, our method is tested on various *in-silico* data while changing the noise parameter values, and its performance is compared with the previous approaches in section 4. In section 5, our method is applied to real-world data collected with wearables, which shows its usefulness in real-world settings. In section 6, we conclude the paper by describing the broad applicability of the method, its some limitations, and potential future work.

2 Background: Previous approaches and the novelty of our approach

As estimation of the state of the circadian clock of an individual is a longstanding challenge, we briefly summarize how our approach is different from previous approaches. Foundational early work done by Brown and colleagues took an initial guess of the state of the circadian clock (e.g., a prior on the circadian phase) and propagated this information forward in time with dynamic (e.g., limit cycle) or simple harmonic mathematical models for the human circadian pacemaker. Then, this propagated information was directly compared with measured data (e.g., time courses of human core body temperature) using Bayesian statistics [7, 8]. Additional statistical models to account for regulation of the systems that produced this data (e.g., temperature or melatonin) were included and standard Kalman filter algorithms were used [6, 9]. Parameters such as the phase and amplitude could be estimated by Markov chain Monte Carlo (MCMC) techniques or minimizing the likelihood, and the variance of these measurements could be found through the resulting distributions or the Fisher information matrix. Such techniques can also be used to distinguish between different models of the circadian clock [7, 8, 27, 28]. As is standard in Kalman filtering algorithms, problems can be divided into two steps, first a time update step where the distributions propagated forward in time with models, and a measurement update step where new measurements are incorporated.

These techniques were used to analyze much of the initial data in the human circadian rhythms field. However, the high computational cost of the likelihood minimization or the distribution calculation caused many of these methods to stop being used. Many studies now use simpler methods (e.g., the time that melatonin collected in dim light crosses a threshold) [33, 60]. However, such methods are not statistical in that they do not calculate confidence intervals for each measurement, nor are they Bayesian in that they do not account for prior or multiple datasets unlike the methods of Brown and colleagues [7, 9].

The most validated models were constructed by Kronauer, Forger, and colleagues and can take in inputs of light measurements in the field or estimates of the light levels to predict the circadian phase at future times [15, 29, 34]. These were compared with measurements of the phase. Subsequent work has shown that models which take in field measurements of activity yield more accurate estimates of the human circadian phase than field measurements of light, perhaps due to activity as an important input into the circadian clock [26]. The models are also directly related and can be thought of as representations of the physiology of the circadian system. For example, biochemical models of the molecular timekeeping of individual cells can be reduced to these models by averaging on approximate manifolds [16]. A recent Ansatz also yield these models from large networks of coupled oscillators [21, 22]. This also explains process noise which has a molecular origin [18] and noise in the inputs to the models [17] as well as the measurement noise considered by Brown and colleagues [7]. We also note that the models have always given continuous measurements of the circadian phase, which can be related to discrete experimental measurements, such as the timing of the core body temperature minimum.

Another framework similar to that by Brown and colleagues is to use particle filters for the time update step [41]. Here, individual stochastic trajectories are simulated similar to the MCMC approach by Brown and colleagues [7]. If a measurement of the phase and its uncertainty is known, it can also be included in a Bayesian framework similar to the work done by Brown and colleagues [7]. One way to do this is to convert the x and x_c variables of these limit cycle models into a geometric phase similar to what is done previously [13, 31, 41] and redistribute the particles to account for the Bayesian statistics. However, the computational costs of this method are also prohibitive in many real-world applications.

Our approach to the time update step is different in that it uses level-set methods [59] to directly calculate the distribution of possible states. Thus, it is built on deterministic simulation rather than running individual stochastic trajectories. Additionally, for the Bayesian measurement update step, we take the approach of phase having units of time rather than thought of as an angle. This is more in line with the averaging method [46] that was used in the creation of the human circadian models and is more accurate since nonlinear models typically do not proceed forward in time at the same angular velocity. Distributions are then updated based on this new time directly without resampling using the measurement update of the LSKF [59], which is the same as that originally proposed in the cubature Kalman filter [2]. Thus, by directly solving for the distributions over time and directly updating the measurement, we can reduce the amount of computational necessity by orders of magnitude, as well as increase the accuracy of simulations. We also show how the magnitude of the noise within these models can be calculated.

3 LSKF framework to estimate the circadian phase and its uncertainty from wearable data

Here, we propose a framework to estimate the circadian phase and its uncertainty based on the LSKF [59] and the Bayesian inference method [4]. This section is organized as follows: In section 3.1, we explain the mathematical models used to define the process equation and the measurement equation of our filtering framework. In section 3.2, the process equation and the measurement equation of our LSKF framework are explained. In section 3.3 and section 3.4, its time-update and measurement-update steps are described, respectively. In section 3.5, we describe how the circadian clock state estimated on the variable domain can be transformed into that on the time domain. In section 3.6, we summarize our method and show an example of its application to clearly explain how it works.

3.1 Mathematical models of the human master circadian pacemaker and the circadian rhythm in heart rate

3.1.1 Limit-cycle oscillator model of the human master circadian pacemaker

The human master circadian pacemaker affected by light can be described by a van der Pol type oscillator model [15]:

$$\frac{dx}{dt} = \frac{\pi}{12}(x_c + B) \quad (2)$$

$$\frac{dx_c}{dt} = \frac{\pi}{12} \left\{ \mu \left(x_c - \frac{4}{3} x_c^3 \right) - x \left(\frac{24}{0.99669\tau_x} \right)^2 + kB \right\} \quad (3)$$

where $\mu = 0.23$, $\tau_x = 24.2$, and $k = 0.55$. The solution trajectory of eq. (2) and eq. (3) is a limit-cycle oscillation representing the endogenous rhythm of the circadian pacemaker. This oscillator is denoted by *Process P*. The B term in eq. (2) and eq. (3) represents the effect of photic drive converted from retinal light exposure on the circadian pacemaker. The conversion of light to the photic drive, denoted by *Process L* is modeled as described below. Light activates photoreceptor activator elements in a “ready” state (fraction $1 - n$) and converts them to a “used” state (fraction n) at a rate of α , which depends on light intensity I eq. (4).

$$\alpha(I) = \alpha_0 \left(\frac{I}{I_0} \right)^p \quad (4)$$

where $\alpha_0 = 0.16$, $p = 0.6$, and $I_0 = 9500$. The used elements are recycled back into the ready state at a rate of $\beta = 0.013$. This is given by

$$\frac{dn}{dt} = 60 \left(\alpha(I)(1 - n) - \beta n \right). \quad (5)$$

As the elements are activated, it generates a drive onto the circadian pacemaker \hat{B} , which is proportional to element flux rate $\alpha(I)(1 - n)$ eq. (6).

$$\hat{B} = G\alpha(I)(1 - n). \quad (6)$$

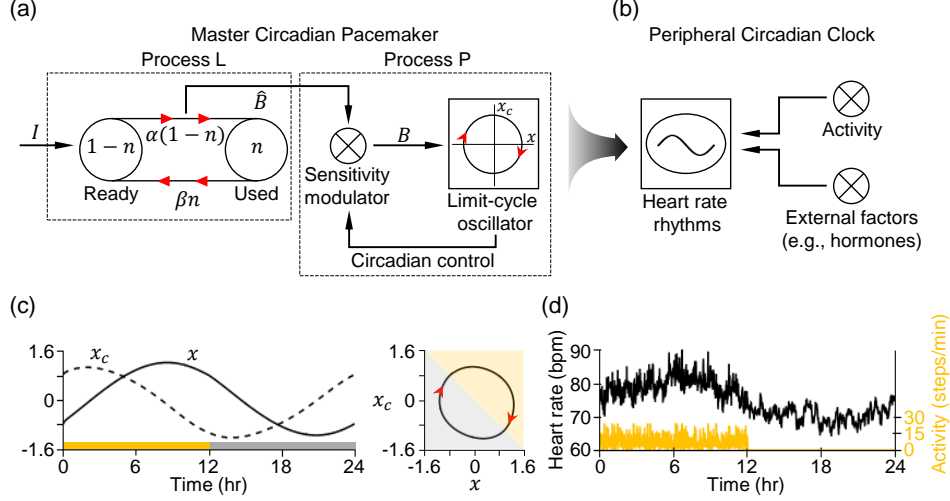


Figure 1. Mathematical models simulating the human circadian timekeeping system. (a,b) Schematic diagram describing the model of the human master circadian clock eq. (2)-eq. (7) (a) and the model of the peripheral circadian rhythm in the heart (b) eq. (8)-eq. (9). (c,d) The exemplary trajectories of x and x_c (c), and HR_t (d). In (c), the light intensity $I(t) = 10000$ lux for $t \in (0, 12)$ and $I(t) = 0$ lux for $t \in (12, 24)$. In (d), the parameter values were adopted from [4].

where $G = 19.875$. The sensitivity of the circadian pacemaker to the drive is modulated in a circadian manner with the state variables x and x_c eq. (7).

$$B = \hat{B}(1 - 0.4x)(1 - 0.4x^c). \quad (7)$$

The model diagram of the master circadian clock and example solution trajectories of x and x_c are shown in Figures 1a and 1c, respectively.

3.1.2 Harmonic-regression-plus-correlated-noise model of the HR circadian rhythm

The circadian rhythm in HR can be described by a harmonic-regression-plus-first-order-autoregressive model with a linear coefficient that corresponds to how much HR increases per activity (step) [4, 40]. Specifically, HR oscillates with an approximately 24 hours period [39], and it increases from this baseline proportionate to activity, matching existing data [49]. Moreover, many external factors, such as cortisol and other hormones [3], stress [10], and caffeine intake [37], affect HR on the hour timescale. This yields a final model for HR at time t , measured in hours:

$$HR_t = \mu - a \cos\left(\frac{2\pi}{\tau}(t - \phi^{HR})\right) + d \cdot Activity_t + v_t \quad (8)$$

where

$$v_t = \alpha \cdot v_{t-\Delta t} + \epsilon_t, \quad (9)$$

μ is the basal HR in beats per minute (BPM), a and ϕ^{HR} are circadian amplitude and phase, respectively, the circadian period $\tau = 24$ in hours, d is the increase in HR per unit activity, $|\alpha| < 1$, and the ϵ_t values are Gaussian random variables with mean zero and variance σ_ϵ^2 . Note that the noise v_t follows the first-order autoregressive noise process eq. (9): the noise at time t carries over a fraction α of the noise at time $t - \Delta t$. This describes the ongoing effects of extrinsic factors on HR. The independent Gaussian noise ϵ_t represents new extrinsic effects and measurement error. The model diagram of the HR rhythm and an example trajectory of HR_t are shown in Figures 1b and 1d, respectively.

3.2 Problem formulation

We consider a continuous-discrete nonlinear filtering model of the circadian timekeeping system whose process equation is formulated with eq. (2)-eq. (7):

$$d\mathbf{x}_t = \mathbf{v}(\mathbf{x}_t)dt + \sqrt{\mathbf{K}}dW_t \quad (10)$$

where

$$\mathbf{x}_t = \begin{pmatrix} x(t) \\ x_c(t) \\ n(t) \end{pmatrix}, \quad \mathbf{v}(\mathbf{x}_t) = \begin{pmatrix} \frac{\pi}{12}(x_c(t) + B) \\ \frac{\pi}{12} \left\{ \mu \left(x_c(t) - \frac{4}{3}x_c^3(t) \right) - x(t) \left(\frac{24}{0.99669\tau_x} \right)^2 + kB \right\} \\ 60 \left(\alpha(I)(1 - n(t)) - \beta n(t) \right) \end{pmatrix},$$

W_t is a standard 3-dimensional Brownian motion, and $\mathbf{K} \in \mathbb{R}^{3 \times 3}$ is a positive semi-definite continuous process noise matrix, with its decomposition $\mathbf{K} = \sqrt{\mathbf{K}}\sqrt{\mathbf{K}}^T$. The phase of the central timekeeping system is indirectly measured from the phase of the peripheral HR clock (i.e., ϕ^{HR} in eq. (8)):

$$\phi_i^{HR} = \phi_i + \phi_{ref} + \epsilon_i^\phi \quad (11)$$

where ϕ_i^{HR} denotes the HR phase on day i , ϕ_i is the phase of the central circadian pacemaker on day i , $\phi_{ref} = -1$ denotes the average difference between the two phases reported in the previous studies [4, 15, 60], and ϵ_i^ϕ is the zero-mean Gaussian measurement noise on day i . For a given day i , we define ϕ_i to be

$$\phi_i = \{t_i \pmod{24} : \mathbb{E}[x(t_i)] \leq \mathbb{E}[x(t)], \forall t \in [24(i-1), 24i]\}. \quad (12)$$

This relationship between the central and peripheral clock states eq. (11)-eq. (12) represents the measurement equation of our filtering framework. The method used to obtain the HR phase estimate from wearable data [4] is described in section 3.4.

3.3 Time-update step

In section 3.3.1, we review the time-update method of the LSKF. In section 3.3.2, we describe how the best possible estimate of \mathbf{x} in eq. (10) can be propagated using the time-update step of the LSKF.

3.3.1 Review of the time-update method of the LSKF

The probability density $u(\mathbf{x}, t)$ of \mathbf{x} in eq. (10) satisfies the Fokker-Plank equation in Ito's calculus [5]:

$$\frac{\partial u(\mathbf{x}, t)}{\partial t} = \frac{1}{2} \nabla \cdot \mathbf{K} \nabla u(\mathbf{x}, t) - \nabla \cdot (\mathbf{v}(\mathbf{x})u(\mathbf{x}, t)). \quad (13)$$

Without loss of generality (WLOG), we may assume the drift function at $\mathbf{x} = 0$ is zero (i.e., $\mathbf{v}(0) = 0$). Then we approximate eq. (13) by taking a linear approximation of \mathbf{v} (i.e., $\mathbf{v}(\mathbf{x}) \approx \mathbf{J}\mathbf{x}$, where \mathbf{J} is the Jacobian matrix):

$$\frac{\partial u(\mathbf{x}, t)}{\partial t} = \frac{1}{2} \nabla \cdot \mathbf{K} \nabla u(\mathbf{x}, t) - \nabla \cdot (\mathbf{J}\mathbf{x}u(\mathbf{x}, t)). \quad (14)$$

An auxiliary function $F(\mathbf{x}, t)$ is introduced to define a level set of a Gaussian distribution as

$$\mathcal{L}(t) := \{\mathbf{x} : F(\mathbf{x}, t) = c\} \quad (15)$$

where $c \in (0, 1)$ is some fixed scalar constant. Note that $\mathcal{L}(t)$ is an ellipsoid if $u(\mathbf{x}, 0)$ is given by a Gaussian function

$$u(\mathbf{x}, 0) = \frac{1}{\sqrt{(2\pi)^d \det \Sigma}} \exp\left(\frac{-\mathbf{x}^T \Sigma^{-1} \mathbf{x}}{2}\right) \quad (16)$$

where d is a dimension of \mathbf{x} , Σ is the covariance matrix, and it is assumed WLOG that \mathbf{x} is centered at 0 at time 0. Since F varies over time, $\mathcal{L}(t)$ propagates in space. To describe its propagation, we consider a velocity of level set $\mathbf{v}_{\mathcal{L}}$ defined by a velocity field satisfying the level-set equation [51]:

$$\frac{\partial F}{\partial t} + \mathbf{v}_{\mathcal{L}} \cdot \nabla F = 0. \quad (17)$$

A velocity of the level set for $\mathcal{L}(0)$ defined in eq. (15) can be explicitly calculated if $u(\mathbf{x}, 0)$ is given by a Gaussian function in eq. (16) [59] as follows:

$$\mathbf{v}_{\mathcal{L}} = \mathbf{J}\mathbf{x} + \frac{1}{2}\mathbf{K}\Sigma^{-1}\mathbf{x}. \quad (18)$$

Using eq. (18), we can show that the solution of a Fokker-Plank equation with linear drift function is a Gaussian distribution if an initial condition $u(\mathbf{x}, 0)$ is given by a Gaussian distribution as follows:

Corollary 1. *A Fokker-Plank equation preserves a Gaussian distribution with a linear drift function eq. (14)*

Proof. eq. (18) is a linear transformation (i.e., a linear velocity field) that instantaneously propagates every level set, independent of the scaling constant c . Since a linear transformation maps Gaussian to Gaussian, the initial Gaussian distribution is mapped to a Gaussian under eq. (18). Hence, $u(\mathbf{x}, t)$, the propagated distribution at time t , is also a Gaussian distribution, and the velocity field $\mathbf{v}_{\mathcal{L}}$ is always well-defined for all t . \square

Note that the proof of corollary 1 is adopted from [59] and corollary 1 can be considered as a corollary of Equation (29) in [30].

We now describe the numerical algorithm for the time-update step. Inspired from corollary 1, we can consider that propagation of a solution of the Fokker-Plank equation with linear drift function for time t eq. (14) is equivalent to tracking its ellipsoid level sets. Hence, we track the movement of the column vectors of \mathbf{M} where $\Sigma = \mathbf{M}\mathbf{M}^T$ since they represent the unique level set for the time update [1]. Specifically, let $\Sigma(0) = \mathbf{M}(0)\mathbf{M}(0)^T$ be the covariance matrix of an initial condition $u(\mathbf{x}, 0)$, and $\mathbf{M}(0) = [\mathbf{x}_1(0) \ \cdots \ \mathbf{x}_d(0)]$ where $\mathbf{x}_i(0)$ is the i -th column vector \mathbf{x}_i of $\mathbf{M}(0)$. Then, we can interpret $\mathbf{x}_i(0)$ as a representative point of one of level sets at time $t = 0$ [59]. It travels at the speed defined by a velocity of level set in eq. (18). Let the position of the propagated points at time t be denoted by $\mathbf{M}(t) = [\mathbf{x}_1(t) \ \cdots \ \mathbf{x}_d(t)]$. Then, $\Sigma(t) = \mathbf{M}(t)\mathbf{M}(t)^T$ is the covariance matrix for the Gaussian that is a solution of eq. (14) at time t because the velocity field defined in eq. (18) is linear and a Gaussian is preserved by a linear transformation. By substituting each column vector of $\mathbf{M}(t)$ for \mathbf{x} in eq. (18) and approximating the Jacobian \mathbf{J} with the central difference in velocity, we obtain

$$\frac{d\mathbf{x}_i(t)}{dt} = \mathbf{v}(\bar{\mathbf{x}} + \mathbf{x}_i) - \frac{1}{2d} \sum_{i=1}^d (\mathbf{v}(\bar{\mathbf{x}} + \mathbf{x}_i) + \mathbf{v}(\bar{\mathbf{x}} - \mathbf{x}_i)) + \frac{1}{2}\mathbf{K}(\mathbf{M}(t)^T)^{-1}e_i \quad (19)$$

where $\bar{\mathbf{x}}$ is the mean of the Gaussian and e_i is the i th unit vector with all entries 0 except for i th entry. The matrix form of eq. (19) is

$$\frac{d\mathbf{M}}{dt} = \mathbf{v}(\bar{\mathbf{x}} + \mathbf{M}) - \frac{1}{2d} \sum_{i=1}^d (\mathbf{v}(\bar{\mathbf{x}} + \mathbf{x}_i) + \mathbf{v}(\bar{\mathbf{x}} - \mathbf{x}_i)) + \frac{1}{2}\mathbf{K}(\mathbf{M}^T)^{-1}. \quad (20)$$

With the averaged velocity (i.e., the second term of eq. (19)), we can also set the velocity of $\bar{\mathbf{x}}$ as follows:

$$\frac{d\bar{\mathbf{x}}}{dt} = \frac{1}{2d} \sum_{i=1}^d (\mathbf{v}(\bar{\mathbf{x}} + \mathbf{x}_i) + \mathbf{v}(\bar{\mathbf{x}} - \mathbf{x}_i)). \quad (21)$$

We concatenate $\bar{\mathbf{x}}$ and \mathbf{M} as a variable $(\bar{\mathbf{x}}|\mathbf{M})$ of $d \times (d + 1)$ dimension and obtain a nonlinear ordinary differential equation (ODE) system. By solving it with any standard ODE solver, we can complete the time-update step between the measurements.

3.3.2 Forward propagation of the estimate of the circadian clock state

Here, we apply the LSKF time-update method to our process equation eq. (10) to propagate the estimate of \mathbf{x} forward until the subsequent measurement is available. Specifically, to track the propagation of the level set by solving eq. (20) and eq. (21), the light intensity I needs to be defined for each time. However, ubiquitous consumer-grade wearable devices typically only record activity measurements instead of light measurements.

To address this problem, Walch et al. proposed a method to convert the activity to light measurements [57]. Then, Huang et al. have recently shown that the ODE model eq. (2)-eq. (7) taking activity as an input instead of light has reasonable accuracy in predicting the circadian phase in multiple clinical datasets [26]. Importantly, activity is better at predicting the phase than light in a shift-worker cohort. We adopted this validated method as follows: The step count (i.e., activity level) measured by wearables at time t denoted by $a(t)$ is converted to the light input I with the piecewise function L eq. (22).

$$L(a(t)) = \begin{cases} 0 \text{ lux} & \text{if } a(t) \leq 0 \\ 100 \text{ lux} & \text{if } a(t) \in (0, 0.1m) \\ 200 \text{ lux} & \text{if } a(t) \in [0.1m, 0.25m) \\ 500 \text{ lux} & \text{if } a(t) \in [0.25m, 0.4m) \\ 2000 \text{ lux} & \text{otherwise} \end{cases} \quad (22)$$

where $m = \frac{\max(a(t))}{2}$. By substituting $L(a(t))$ for $I(t)$ in eq. (10) and solving eq. (20) and eq. (21), we can compute the propagation of \mathbf{x} until a new measurement is available, which is shown as black circles in Figure 2a. This allows the prediction of the circadian clock state on day $i + 1$ when measurements until day i are given (i.e., $\mathbf{x}_{i+1|i} \sim N(\bar{\mathbf{x}}_{i+1|i}, \Sigma_{i+1|i})$), which is shown as a blue circle in Figure 2a.

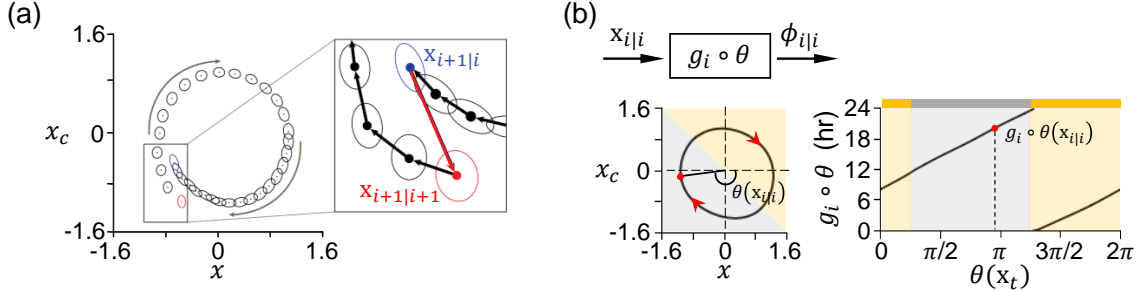


Figure 2. Key steps of our Kalman filter framework. (a) Graphical illustration of the time-update step and the measurement-update step. By the time-update method, the ellipsoid level set of \mathbf{x} represented as a circle is propagated forward (black), and the circadian clock state is predicted (blue). The predicted state is updated by the measurement-update method (red). (b) Transformation of the clock state from the variable domain to the time domain.

3.4 Measurement-update step

In section 3.4.1, we review the measurement-update method used in the LSKF. In section 3.4.2, we describe how the estimate of \mathbf{x} in eq. (10) is updated using the method when the subsequent measurement is given.

3.4.1 Review of the measurement-update of the LSKF

For the measurement-update, the method from the square root continuous-discrete cubature Kalman filter [2, 59] is used. The method was adopted because it can accommodate a positive semi-definite matrix \mathbf{M} calculated in the LSKF time-update step, which is required for the reliability of the method [2, 59]. Because our notations are different from those used in [2, 59], we restate the measurement-update algorithm in Algorithm 1.

3.4.2 Update of the estimate of the circadian clock state with wearable measurements

Here, we describe how the predicted estimate of $\mathbf{x}_{i+1|i}$ in section 3.3.2 is updated with wearable data. First, we extracted the HR phase on each day i (i.e., ϕ_i^{HR} in eq. (11)), which is the measurement of our filtering problem, from HR and activity data collected with wearables. Specifically, we fit eq. (8) to the HR and

Algorithm 1 Measurement-update step

Require: Predicted mean after the time-update step $\bar{\mathbf{x}}$, a factorization of the predicted covariance matrix after the time-update step \mathbf{M} such that $\Sigma = \mathbf{M}\mathbf{M}^T$, measurement \mathbf{z} , a factorization of measurement noise matrix $\sqrt{\mathbf{R}}$, and a measurement function \mathbf{h}

- 1: Find the concatenated matrix of the cubature points

$$\mathbf{N} = \bar{\mathbf{x}} + \sqrt{2d}(\mathbf{M}| - \mathbf{M}), \quad (23)$$

by applying a vector-matrix addition to $\bar{\mathbf{x}}$ and each column of the concatenated matrix $(\mathbf{M}| - \mathbf{M})$. Note that \mathbf{N} is a $d \times 2d$ matrix if $\bar{\mathbf{x}}$ is a $d \times 1$ matrix.

- 2:

- 3: Evaluate the measurement function \mathbf{h} on each column of \mathbf{N} to compute the propagated cubature points as follows:

$$\mathbf{Z} = \mathbf{h}(\mathbf{N}). \quad (24)$$

Note that \mathbf{Z} is $1 \times 2d$ matrix if \mathbf{h} is a scalar-valued function.

- 4: Estimate the predicted measurement from the propagated cubature points.

$$\bar{\mathbf{z}} = \frac{1}{2d} \sum_{i=1}^{2d} \mathbf{Z}_i, \quad (25)$$

where \mathbf{Z}_i is the i th column of \mathbf{Z} .

- 5: Perform the QR-factorization to obtain matrix \mathbf{T}_{11} and \mathbf{T}_{21}

$$\begin{pmatrix} \mathbf{T}_{11} & \mathbf{O} \\ \mathbf{T}_{21} & \mathbf{T}_{22} \end{pmatrix} = \text{qr} \begin{pmatrix} \mathbf{Z} & \sqrt{\mathbf{R}} \\ \mathbf{N} & \mathbf{O} \end{pmatrix}, \quad (26)$$

where \mathbf{O} is a zero matrix of appropriate size, such that the QR factorization can be performed.

- 6: Use a backward stable solver to compute the cubature gain \mathbf{W} such that

$$\mathbf{T}_{21} = \mathbf{W}\mathbf{T}_{11} \quad (27)$$

- 7: Use the computed cubature gain \mathbf{W} to estimate the corrected mean

$$\hat{\mathbf{x}} = \bar{\mathbf{x}} + \mathbf{W}(\mathbf{z} - \bar{\mathbf{z}}) \quad (28)$$

- 8: Estimate a factorization of the corrected covariance matrix

$$\hat{\mathbf{M}} = \mathbf{T}_{22} \quad (29)$$

return The corrected mean $\hat{\mathbf{x}}$ and a factorization of the corrected covariance matrix $\hat{\mathbf{M}}$

activity data using the recently developed Bayesian inference framework [4] that is based on Goodman and Weare's affine-invariant MCMC algorithm, which prevents potential bias from large gaps in wearable data [20]. This returns the mean and variance of the HR phase estimate computed from its posterior distribution on day $i + 1$. We use them as the measurement ϕ_{i+1}^{HR} in eq. (11) (i.e., \mathbf{z} in Algorithm 1) and the measurement noise ϵ_{i+1}^ϕ in eq. (11) (i.e., \mathbf{R} in Algorithm 1). This allows implementation of the measurement-update method with the measurement equation eq. (11) denoted by \mathbf{h} in Algorithm 1. This updates $\mathbf{x}_{i+1|i}$ predicted by the time-update method and returns the corrected estimate $\mathbf{x}_{i+1|i+1} \sim N(\bar{\mathbf{x}}_{i+1|i+1}, \Sigma_{i+1|i+1})$, which is shown as a red circle in Figure 2a. This can be transformed into the estimate $\phi_{i+1|i+1}$ on the time domain (see section 3.5 below for details).

3.5 Transformation of the circadian clock state estimate from the variable domain to the time domain

Our method estimates the circadian clock state $\mathbf{x}_{i|i} \sim N(\bar{\mathbf{x}}_{i|i}, \Sigma_{i|i})$. Here, we describe how the estimated distribution can be transformed from the variable domain to the time domain. We first define a function $\theta(\mathbf{x})$ to establish a relationship between the state vector \mathbf{x} and the angle formed by the projection of \mathbf{x} on the (x, x_c) -plane with the origin as follows:

$$\theta(\mathbf{x}) = \begin{cases} -\arctan\left(\frac{x_c}{x}\right) & \text{if } x \geq 0, x_c \leq 0 \\ \pi - \arctan\left(\frac{x_c}{x}\right) & \text{if } x < 0 \\ 2\pi - \arctan\left(\frac{x_c}{x}\right) & \text{if } x \geq 0, x_c > 0 \end{cases} \quad (30)$$

Then, we construct an interpolation function $g_i : [0, 2\pi] \rightarrow [t_i, t_{i+1}]$ that relates $\theta(\mathbf{x}_t)$ to time t where t_i and t_{i+1} is the midnight (00:00 am) of day i and day $i + 1$, respectively, using the trajectory of \mathbf{x} on day i obtained by propagating it with the level-set method. Finally, the composition $(g_i \circ \theta)(\mathbf{x}_t)$ allows us to relate \mathbf{x}_t to t during day i . As a result, we can obtain the circadian clock state on the time domain eq. (31) as shown in Figure 2b.

$$\phi_{i|i} = (g_i \circ \theta)(\mathbf{x}_{i|i}) \quad (31)$$

where $\mathbf{x}_{i|i} \sim N(\bar{\mathbf{x}}_{i|i}, \Sigma_{i|i})$. To sample from the nonlinearly transformed random variable $\phi_{i|i}$, we used a Monte Carlo approach: we took a large number of N random samples from $\mathbf{x}_{i|i} \sim N(\bar{\mathbf{x}}_{i|i}, \Sigma_{i|i})$, and computed their transformed values that are N samples of $\phi_{i|i}$.

3.6 Summary of the filtering algorithm and an example of its application

Our filtering framework can be illustrated in Figure 3a. We predict the estimate on day $i + 1$, $\mathbf{x}_{i+1|i}$, from prior knowledge $\mathbf{x}_{i|i}$ as described in section 3.3. Then, it is updated with ϕ_{i+1}^{HR} extracted by applying the Bayesian method [4] to wearable data on day $i + 1$ as described in section 3.4. This returns the estimate $\mathbf{x}_{i+1|i+1}$ that is transformed into the estimate on the time domain $\phi_{i+1|i+1}$, as described in section 3.5. By iterating this procedure, we can estimate the phase on each day in a consecutive manner. This can be summarized as Algorithm 2.

To clearly illustrate how our algorithm works, we applied it to *in-silico* data and showed its estimation results. Specifically, we first created a virtual scenario mimicking a typical human lifestyle: a virtual subject sleeps from 23hr to 7hr and regularly acts during the waking time, as described in Figure 3b. The simulated HR rhythm becomes minimum at the midpoint of sleep (i.e., the true HR phase = 3hr) following the previous work [4], and the true internal phase of the central pacemaker on day i $\phi_i^{true} = 4\text{hr}$. From these activity and HR data, the evolution of posterior distributions of the internal circadian phase $\phi_{i|i}$ can be generated by our method, as shown in Figure 3c. In Figure 3c, a guess of the initial mean state $\bar{\mathbf{x}}_{t_0}$ was completely wrong. Moreover, a guess of the initial covariance matrix of \mathbf{x} $\Sigma(t_0)$ was set to be large so that initial priors were not highly informative, resulting in the broad distribution on day 1. Despite this circumstance, our method can accurately estimate the internal circadian phase after a few days, as shown in Figure 3c and 3d.

Algorithm 2 Kalman filtering for the circadian phase estimation

Require: A guess of initial mean state $\bar{\mathbf{x}}_{t_0}$ at time t_0 , a factorization of a guess of covariance matrix $\mathbf{M}(t_0)$, the HR phase estimates $\phi_1^{HR}, \dots, \phi_n^{HR}$ and its estimate errors $\epsilon_1^\phi, \dots, \epsilon_n^\phi$, on day $1, \dots, n$

- 1: **for** day i from day 1 to day n **do**
 - 2: Time-update: solve eq. (20) and eq. (21) with initial conditions $\bar{\mathbf{x}}_{i-1|i-1}$ and $\mathbf{M}_{i-1|i-1}$ such that $\Sigma_{i-1|i-1} = \mathbf{M}_{i-1|i-1} \mathbf{M}_{i-1|i-1}^T$ from $t = \phi_{i-1|i-1}$ to $t = \phi_{i|i-1}$ using a numerical ODE solver to obtain $\mathbf{x}_{i|i-1} \sim N(\bar{\mathbf{x}}_{i|i-1}, \Sigma_{i|i-1})$.
 - 3: Measurement-update: perform Algorithm 1 with $\bar{\mathbf{x}}_{i|i-1}$, $\mathbf{M}_{i|i-1}$, ϕ_i^{HR} , and $\sqrt{\epsilon_i^\phi}$, and the measurement function eq. (11) to compute $\mathbf{x}_{i|i} \sim N(\bar{\mathbf{x}}_{i|i}, \Sigma_{i|i})$.
 - 4: Transformation into the time domain: $\phi_{i|i} = (g_i \circ \theta)(\mathbf{x}_{i|i})$ where $\mathbf{x}_{i|i} \sim N(\bar{\mathbf{x}}_{i|i}, \Sigma_{i|i})$
 - 5: **return** $\phi_{i|i}$
-

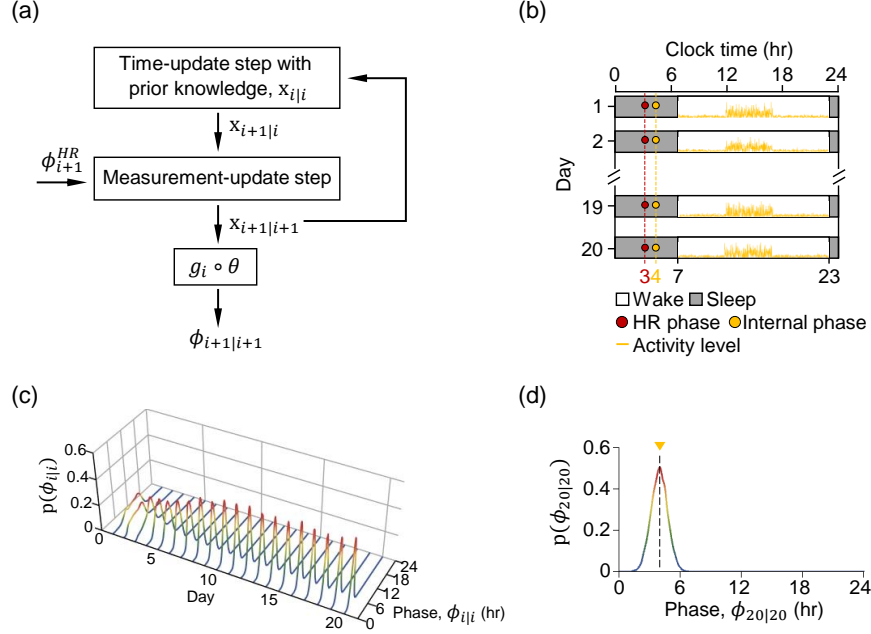


Figure 3. Kalman filtering for the circadian phase estimation. (a) Diagram describing the Kalman filter to estimate the evolution of the posterior distributions of the internal circadian phase $\phi_{i|i}$. (b) A simulated scenario that captures a typical lifestyle. Sleep offset and onset times were set as 7hr and 23hr, respectively. The wake and sleep times are represented as white and black box. Activity level $a(t)$ in eq. (22) is denoted by yellow line. The HR phase and the internal phase were set as 3hr and 4hr, respectively. Please see Scenario 1 described in section 4.1 and Table 1 for more details. (c) The evolution of the posterior distributions of $\phi_{i|i}$ over days. Here, a guess of $\bar{\mathbf{x}}_{t_0}$ was set as $[x(t_0), x_c(t_0), n(t_0)] = [1, 0, 0.5]$ that is completely different to the true $[-0.61, -0.76, 0.34]$. A guess of $\Sigma(t_0)$ was set as $0.1 \cdot I$ and $K = 10^{-2} \cdot I$ where I is the identity matrix of order 3. (d) The posterior distribution on the last day (i.e., $\phi_{20|20}$). The triangle and dashed line represent the true internal phase $\phi_i^{true} = 4$ hr.

4 Numerical study

Here, we perform a series of numerical experiments to study the usefulness of our method. This section is structured as follows: In section 4.1, we investigate the relationship between the process noise \mathbf{K} in the circadian clock and the phase estimate, which is impossible with previous methods [26, 52, 61]. In section 4.2, we show that our method has an overall performance improvement over previous methods [26, 4].

4.1 Relationship between the process noise and the phase estimate

The circadian clock state \mathbf{x} is influenced by noise from various sources [55]. For instance, stochastic biochemical reactions occurring in the circadian clock and many biological systems interacting with the circadian clock, such as a metabolic system, cause the randomness of the clock state. This can be described with the process noise matrix \mathbf{K} eq. (10) of the form

$$\mathbf{K} = \begin{pmatrix} \sigma_P^2 & 0 & 0 \\ 0 & \sigma_P^2 & 0 \\ 0 & 0 & \sigma_L^2 \end{pmatrix} \quad (32)$$

where σ_P represents the magnitude of the noise directly affecting the master clock (*Process P* in Figure 1a) and σ_L represents the magnitude of the noise in the biological process (*Process L* in Figure 1a) that transmits the external light signal from the retina to the master clock via the retinohypothalamic tract.

Here, we studied the relationship between the process noise in the circadian clock and the phase estimate using our filtering algorithm. We first generated *in-silico* data mimicking the typical human lifestyle

illustrated in Figure 3b. We set the sleep offset time t_i^{off} and onset time t_i^{on} of day i as 7am and 11pm, respectively, so that activity level on day i $a_i(t) = 0$ if $t \in [0, t_i^{\text{off}}) \cup [t_i^{\text{on}}, 24]$. We next defined $a_i(t)$ in wake time $[t_i^{\text{off}}, t_i^{\text{on}})$ as done in previous work [12, 41]. Specifically, we subdivided the wake time into three stages: morning $[t_i^{\text{off}}, t_i^{\text{off}} + 5)$, afternoon $[t_i^{\text{off}} + 5, t_i^{\text{off}} + 10)$, and evening $[t_i^{\text{off}} + 10, t_i^{\text{on}})$. Then, under the assumption that level of external signals (e.g., light or activity) is low in the morning, high in the afternoon, and again low in the evening like the change of light intensity during the course of a day, $a_i(t)$ was set as

$$a_i(t) = \begin{cases} \max(\mu_l + N(0, \sigma_l^2), 0) & \text{if } t_i^{\text{off}} \leq t < t_i^{\text{off}} + 5 \\ \max(\mu_h + N(0, \sigma_h^2), 0) & \text{if } t_i^{\text{off}} + 5 \leq t < t_i^{\text{off}} + 10 \\ \max(\mu_l + N(0, \sigma_l^2), 0) & \text{if } t_i^{\text{off}} + 10 \leq t < t_i^{\text{on}} \\ 0 & \text{otherwise} \end{cases} \quad (33)$$

where μ_l and σ_l denote the mean and the standard deviation of the low activity level, respectively, and μ_h and σ_h denote the mean and the standard deviation of the high activity level, respectively. We took $a_i(t)$ as the maximum between a sample from $\mu + N(0, \sigma^2)$ and 0 to prevent it from being negative. Note that we set μ_l and μ_h as 5 steps/min and 25 steps/min, respectively, with which the activity signal is converted on average to a typical ordinary (500 lux) - bright (2000 lux) - ordinary (500 lux) light exposure by eq. (22). Under this activity setting, we simulated the HR rhythm with a nadir at the midpoint of sleep 3am using the model eq. (8) based on the previous study [4]. Then, we finally defined the internal phase of the central pacemaker ϕ_i^{true} to be 4am based on its relationship with the HR phase eq. (11). More details of the simulated setting named Scenario 1 are given in Table 1.

We applied our method to Scenario 1 and analyzed the estimates with the two quantities, root-mean-squared (RMSE) and non-coverage rate (NCR). The RMSE is the standard deviation of the difference between the mean phase estimate $\bar{\phi}_{i|i}$ and the true phase ϕ_i^{true} , which is defined to be

$$RMSE = \sqrt{\frac{1}{N} \sum_{i=1}^N e_i^2} \quad (34)$$

where $e_i = |\mathbb{E}[\phi_{i|i}] - \phi_i^{\text{true}}|$ and N is the total number of days that the phase was estimated. The NCR is the rate of days that the true phase is not included in the 95% credible interval, which is defined to be

$$NCR = 1 - \frac{1}{N} \sum_{i=1}^N \mathbb{1}_{\text{CI}}^i(\phi_i^{\text{true}}) \quad (35)$$

where $\mathbb{1}_{\text{CI}}^i$ denotes the indicator function that maps inputs to one if they are included in the 95% credible interval on day i . The graphical illustration of the RMSE and the NCR is shown in Figure 4a. The small value of both the RMSE and the NCR means that both the mean and the uncertainty of the phase estimate are accurately identified. This interpretation of the relationship between the two quantities and the phase estimate is shown in Figure 4b.

Using these two measures, we analyzed the phase estimates obtained by applying our method to Scenario 1. Specifically, we first let $\sigma_L = 0$ and took \mathbf{K} of the form eq. (36) to focus on exploring the relationship between the phase estimate and the noise directly affecting the central pacemaker (i.e., the noise in *Process P*). Then, we varied

$$\mathbf{K} = \begin{pmatrix} \sigma_P^2 & 0 & 0 \\ 0 & \sigma_P^2 & 0 \\ 0 & 0 & 0 \end{pmatrix}. \quad (36)$$

σ_P of eq. (36) and calculated the RMSE and the NCR as shown in Figure 4c. In Figure 4c, small σ_P results in the small RMSE but the large NCR. This indicates that ruling out the noise in the central pacemaker might cause problems related to estimating the phase uncertainty. On the other hand, when σ_P is set to be large, the NCR is small, but the RMSE is large, showing that overrating σ_P can lead to an inaccurate estimation of the mean phase. Accordingly, σ_P of appropriate magnitude is required for accurate estimation of both the mean and the uncertainty of the phase. We similarly analyzed the relationship between the phase

Parameters	Summary of Scenarios		
	Scenario 1	Scenario 2	Scenario 3
<i>Activity level</i>			
morning & evening μ_l	5 steps/min	5 steps/min	5 steps/min
afternoon μ_h	25 steps/min	25 steps/min	25 steps/min
sleep	0 steps/min	0 steps/min	0 steps/min
<i>Activity uncertainty</i>			
σ_l	7.5 steps/min	7.5 steps/min	7.5 steps/min
σ_h	30 steps/min	30 steps/min	30 steps/min
σ_s	0 steps/min	0 steps/min	2 steps/min
σ_t	0 hrs	1.5 hrs	1.5 hrs
HR phase	3hr	3hr	3hr
Internal phase	4hr	4hr	4hr
<i>HR signal</i>			
μ	70 bpm	70 bpm	70 bpm
a	4 bpm	4 bpm	4 bpm
ϕ^{HR}	3hr	3hr	3hr
d	0.3	0.3	0.3
<i>HR uncertainty</i>			
σ_ϵ	3 bpm	3 pm	7 bpm
α	0.9	0.9	0.95

Table 1. Summary of the simulated scenarios. In Scenario 1, the randomness of activity level in wake time is only considered. In Scenario 2, the randomness of the sleep onset and offset times is also considered. In scenario 3, the small randomness of activity level in sleep time, due to tossing and turning or measurement noise of wearables, for example, is additionally considered. Moreover, the HR uncertainty is increased to account for the potentially large measurement errors in wearable HR data in real-world settings.

estimate and the noise in the light processor (i.e., the noise in *Process L*) with \mathbf{K} of the form

$$\mathbf{K} = \begin{pmatrix} 0 & 0 & 0 \\ 0 & 0 & 0 \\ 0 & 0 & \sigma_L^2 \end{pmatrix}. \quad (37)$$

Although σ_L changes, the RMSE and the NCR remain small and large, respectively, as shown in Figure 4d, again indicating that the noise in *Process P* needs to be considered for accurate phase estimation. Moreover, the weak dependence of the RMSE and the NCR on σ_L suggests that the noise in *Process L* affects the state of the central pacemaker more weakly than that in *Process P*. This is supported by the fact that the noise in *Process L* originated from the light signal transduction pathway (not the central clock), so it indirectly affects the central clock state. To study this, we explored the association of the phase estimate with the total noise in *Process P* and *Process L* by taking \mathbf{K} of the form

$$\mathbf{K} = \sigma_{\mathbf{K}}^2 \cdot I \quad (38)$$

where $\sigma_{\mathbf{K}}$ denotes the magnitude of the total noise, and I is the identity matrix of order 3. As expected, the relationship between the phase estimate and the total process noise shown in 4e is mainly determined by the influence of the noise in *Process P* shown in Figure 4c. These results obtained using our method provide an understanding of the relationship between the circadian phase and noise in the central pacemaker, which is experimentally unobservable. Importantly, based on this knowledge, we can infer the magnitude of the process noise that accurately describes the mean and the uncertainty of the circadian phase, leading to both

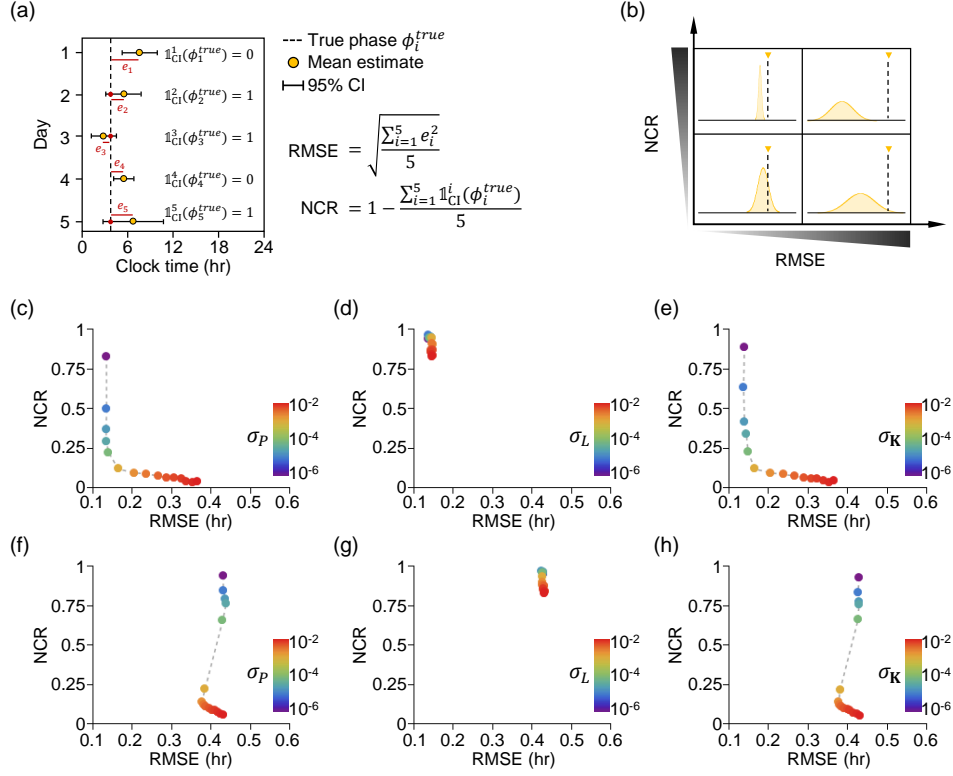


Figure 4. The association of the circadian phase estimate with the noise in the circadian system. (a) The schematic illustration of the definition of the RMSE and the NCR. (b) The relationship of the phase estimate with the RMSE and the NCR. (c-h) The change of the RMSE and the NCR upon the noise magnitude in Scenario 1 (c-e) and in Scenario 2 (f-h). In (c) and (f), only the noise in *Process P* (i.e., σ_P) was considered. In (d) and (g), only the noise in *Process L* (i.e., σ_L) was considered. In (e) and (h), the two noises were considered together.

the small RMSE and NCR. For example, from Figure 4e, we can figure out that σ_K yielding both the small RMSE (0.164hr) and NCR (0.047) is 10^{-3} in Scenario 1.

We next applied our method to more realistic *in-silico* data named Scenario 2. In Scenario 2, the settings of Scenario 1 are replicated except that uncertainty is introduced into sleep offset time t_i^{off} and onset time t_i^{on} as follows:

$$t_i^{\text{off}} \sim 7 + N(0, \sigma_t^2), \quad t_i^{\text{on}} \sim 23 + N(0, \sigma_t^2) \quad (39)$$

where $\sigma_t = 1.5\text{hr}$ represents the uncertainty of the sleep onset and offset times (see Table 1 for more details). Figures 4f, 4g, and 4h describe the association of the phase estimate with the noise in *Process P*, the noise in *Process L*, and the total noise, respectively, in Scenario 2, like Figures 4c, 4d, and 4e. In Scenario 2, the relationship between phase estimate and noise is mainly governed by noise in *Process P*, as in Scenario 1. However, unlike Scenario 1, the change of the RMSE upon the addition of σ_P is not large, indicating the discrepancy of the circadian dynamics in different sleep/wake patterns.

We finally analyzed the most challenging but realistic *in-silico* data named Scenario 3. In Scenario 3, the settings of Scenario 2 are repeated except that the randomness of activity level in sleep time, which originated from small unconscious movements during sleep and measurement noise of wearables, is introduced as follows:

$$a_i(t) = \max(N(0, \sigma_s^2), 0) \quad \text{if } 0 \leq t < t_i^{\text{off}} \text{ or } t_i^{\text{on}} \leq t \leq 24 \quad (40)$$

where $\sigma_s = 2$ steps/min represents the magnitude of the small randomness of activity level in sleep time. Moreover, we increased the uncertainty of HR measurements to account for the potentially large measurement noise in HR data collected in real-world settings reported on [4]. See Table 1 for more details. Figures 5a,

5b, and 5c present the association of the phase estimate with the noise in *Process P*, the noise in *Process L*, and the total noise, respectively, in Scenario 3, like Figure 4. As in Scenario 1 and 2, the relationship is mainly determined by the noise in *Process P*. However, unlike the other scenarios, the RMSE and the NCR are very large even if σ_P is small, as shown in Figure 5a. Moreover, unlike Scenario 1, the RMSE is large when only the noise in *Process L* is considered as shown in Figure 5b. This indicates that the noise in *Process P* needs to be necessarily considered in realistic settings to estimate both the mean and uncertainty of the phase accurately. Importantly, even in this challenging scenario, our method can estimate the phase within 1hr (i.e., $\text{RMSE} < 1\text{hr}$) with a carefully chosen $\sigma_K = 6 \cdot 10^{-3}$ as highlighted by an arrow in Figure 5c, which is impossible with the previous methods [26, 4] (see section 4.2 below for more details).

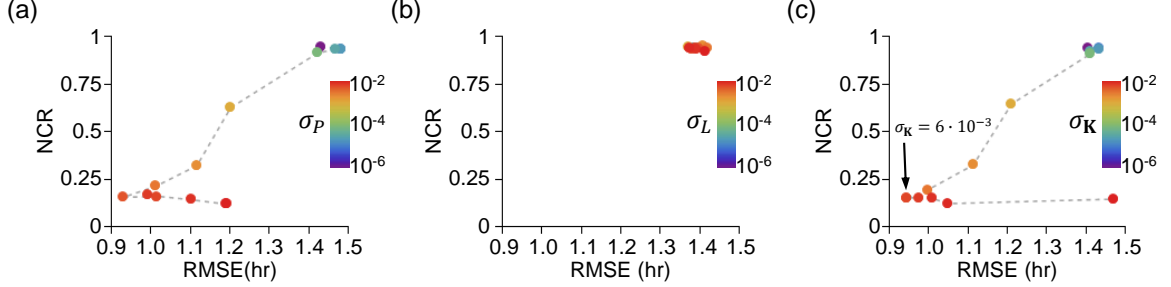


Figure 5. The association of the circadian phase estimate with the noise in the circadian system in the scenario is the most realistic among the others. (a-c) The change of the RMSE and the NCR upon the noise magnitude in Scenario 3. In (a), only the noise in *Process P* was considered. In (b), only the noise in *Process L* was considered. In (c), the two noises were considered together.

4.2 Performance comparison

Here, we compared the performance of our LSKF method with the recently developed methods to demonstrate its capabilities for tracking the circadian phase from wearable data. Specifically, two previous methods were adopted for the comparison. The first previous method proposed in [26] tracks the circadian phase based solely on the mathematical model of the human circadian clock eq. (10) that takes activity wearable data as an input as we described in section 3.3.2. The second one directly calculates the central pacemaker phase from the HR phase estimated by the Bayesian method [4] based on their relationship eq. (11) (i.e., $\phi_i = \phi_i^{HR} - \phi_{ref}$). These two methods were chosen for the comparison study for the following reasons: (i) they are recently developed and thus sophisticated; (ii) our LSKF method integrates the prediction from the model used in [26] with the physiological parameter (i.e., the HR phase) obtained using the method in [4]. We applied the methods to the *in-silico* data of Scenario 3, which is the most realistic but challenging setting and calculated the absolute error (i.e., e_i in eq. (34)) and the standard deviation (i.e., the uncertainty) of the estimate on each day. Then, we compared them with the ones calculated with our LSKF method. Figures 6a, 6b, and 6c show the evolution of the posterior distributions of the phase over days estimated using our LSKF method, the model prediction [26], and the HR measurements [4], respectively. They show that the distributions computed using our method are narrower than those obtained using other methods. Moreover, the filtering algorithm is more accurate than the previous methods, as shown in Figures 6d. Indeed, the absolute error and the uncertainty of our method are smaller than those of the others, as shown in Figures 6e and 6f. Most importantly, our method can estimate the phase within 1hr ($\text{RMSE} = 0.942\text{hr}$) while the others cannot (model prediction: $\text{RMSE} = 1.996\text{hr}$ and HR measurement: $\text{RMSE} = 1.527\text{hr}$).

We next investigated whether the outperformance of our method is preserved even if the magnitude of the process noise σ_K changes. Specifically, in Figures 6e and 6f, $\sigma_K = 6 \cdot 10^{-3}$ was used because it allows our method to accurately capture the dynamics of the circadian systems, resulting in the phase estimation with the small RMSE and NCR in Scenario 3 as shown in Figure 5c. Importantly, even if this σ_K varies, and thus the performance of our method becomes worse, its RMSE is overall smaller than the RMSE of the previous methods, as presented in Figure 6g. In particular, the RMSE of our method is always smaller than that of the method based solely on the model prediction. Moreover, the NCR of our method is comparable

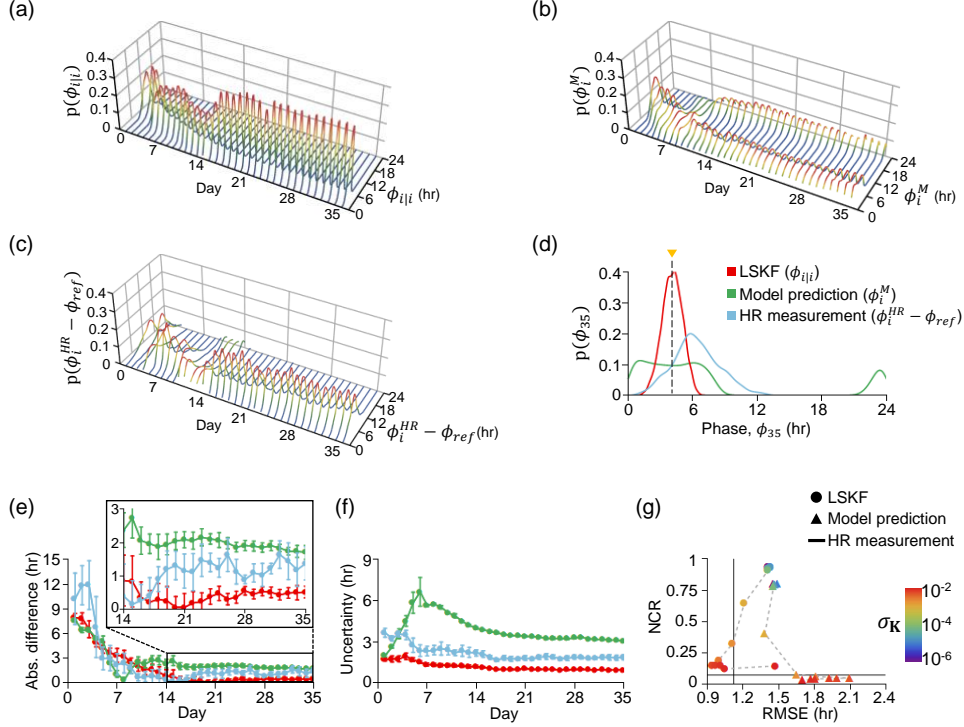


Figure 6. Our filtering approach integrating the model prediction with the physiological proxies can improve the accuracy of the circadian phase estimation from wearable measurements. (a-c) The evolution of the posterior distributions of the phase, obtained using our LSKF method (a), solely based on model prediction (b) or by direct calculation from the HR phase (c). Here, the three methods were applied to Scenario 3 and σ_K of $\mathbf{K} = \sigma_K \cdot \mathbf{I}$ set as $6 \cdot 10^{-3}$ because it allows for accurately capturing the circadian dynamics in Scenario 3 as shown in Figure 5c. (d) The posterior distributions estimated by the three methods on the last day. (e) The absolute difference between the true phase and the mean phase estimate over days. Here, five independent *in-silico* data of Scenario 3 were analyzed by the methods, and the five computed absolute differences were averaged. The error bar denotes the standard error of the mean (SEM). (f) The phase uncertainty (i.e., the standard deviation of the phase estimate) over days. The mean and SEM of the phase uncertainties on each day were calculated as in (e). (g) The RMSE and the NCR of the three methods are computed with various σ_K . Note that the estimation result of the method that directly calculates the master clock phase only from the HR phase is independent of σ_K . Thus, the RMSE and the NCR of the method are represented as the vertical and horizontal lines, respectively.

with that of the previous methods with a carefully selected σ_K . These results demonstrate the benefits of the filtering approach on the circadian phase estimation from wearable data.

5 Application to a real data set

To demonstrate our phase tracking algorithm on a real data set, we used real-world wearable-device data that has been reported in [4]. In this study, the activity and HR measurements were collected in real-life settings with wearables. We analyzed the data from one subject and demonstrated the usefulness of our algorithm in Figure 7. Specifically, using our filtering method, we estimated the circadian phases, and they were compared with the phases that were predicted based solely on the mathematical model taking activity as an input as the previous studies did [26, 52, 61]. We also compared our estimates with those directly calculated from the HR phases obtained using [4]. Figures 7a, 7b, and 7c show the phases estimated by our method, the predicted phases by the mathematical model, and the phases directly calculated from the HR phases, respectively. In their left panels, the evolution of the posterior distributions of the phase is

presented. The distributions on the last day are presented in Figure 7d. In the right panels of Figures 7a, 7b, and 7c, the mean and the standard deviation of the distributions are shown with double-plotted actograms. The standard deviation representing the uncertainty of the phase estimate is quantified in Figure 7e. These figures show that the posterior distributions computed using our LSKF method are narrower than the others. Figure 7f shows that this pattern is preserved even if the magnitude of the process noise $\sigma_{\mathbf{K}}$ is varied so that the noise magnitude leading to the best performance of our method is not exploited in the estimation. This indicates that the uncertainty of the phase estimate can be reduced when combining the model prediction and the measurements from wearables, which is consistent with our results in the numerical experiments. Moreover, the phase estimated by our method differs from the others, for example, as shown in Figure 7d. Considering this with the outperformance of our method in the numerical study, filtering approaches like our algorithm might be needed for accurate circadian phase estimation.

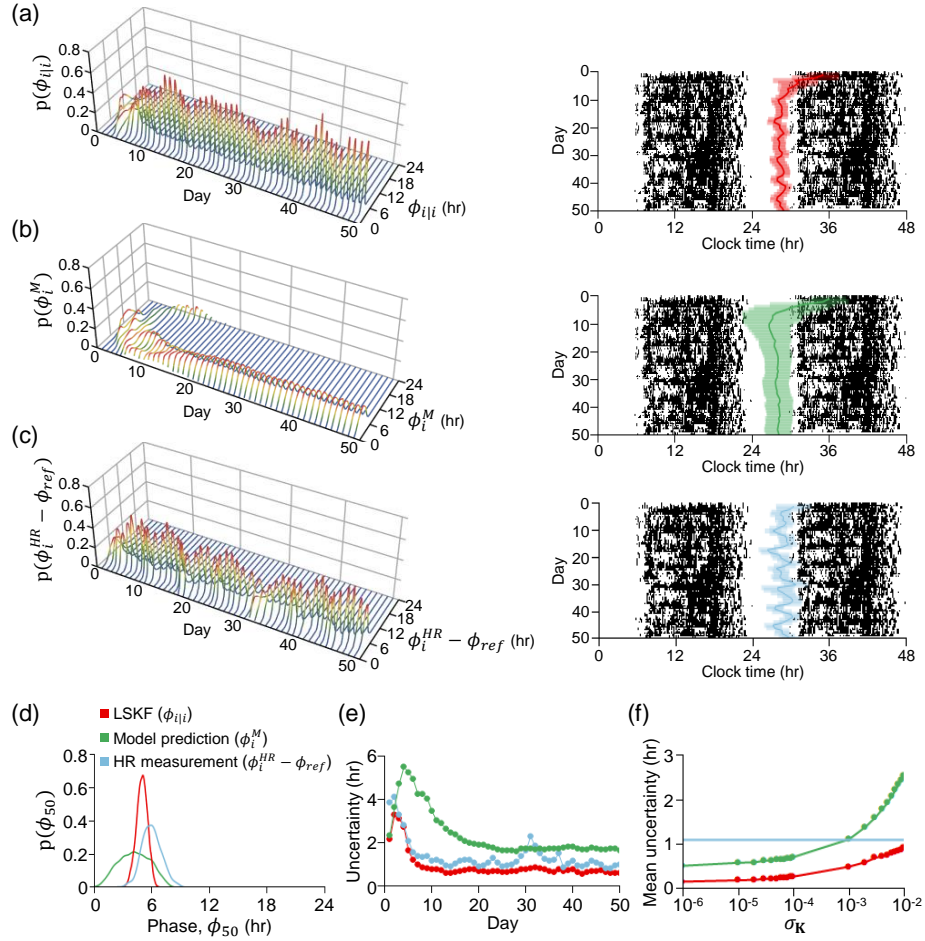


Figure 7. Estimation of the circadian phase from real-world wearable-device data. (a-c) The phase estimates obtained using our filtering method (a), solely based on model prediction (b), or by direct calculation from the HR phase (c). In the left panel, the evolution of the posterior distributions of the phase is presented. In the right panel, their mean and standard deviation are plotted together with actograms. Here, $\sigma_{\mathbf{K}}$ of $\mathbf{K} = \sigma_{\mathbf{K}} \cdot \mathbf{I}$ set as $6 \cdot 10^{-3}$ that allows the accurate identification of the circadian dynamics in Scenario 3 as shown in Figure 6c. (d) The posterior distributions estimated by the three methods on the last day. (e) The phase uncertainty over days. (f) The average of the phase uncertainties over days that is computed with various $\sigma_{\mathbf{K}}$. Note that the estimation result of the method that directly calculates the master clock phase only from the HR phase is independent of $\sigma_{\mathbf{K}}$. Thus, the uncertainty computed using the method is constant over $\sigma_{\mathbf{K}}$.

6 Conclusions

We developed a Kalman filter framework for estimating the circadian phase. It integrates the peripheral clock phase extracted from wearable data with the master clock phase predicted from the mathematical model. As well as estimating the phase, our method can quantify its uncertainty systematically, which is impossible with the previous methods based on ODE models [26, 52, 61]. Numerical experiments in Figure 6 showed how much the uncertainty could be reduced when utilizing the indirect observation (i.e., the HR phase) of the master clock state. Moreover, our method overall outperforms the previous methods, [4, 26, 40] as presented in Figure 6. These results suggest new avenues for exploiting noninvasive wearable data for chronotherapy in free-living conditions.

In addition to its accuracy, our framework can successfully minimize the influence of initial conditions on the phase estimation. Our method continuously updates the phase estimate by the measurement-update step described in section 3.4.2. This results in the rapid identification of the true phase even if arbitrary initial conditions are given, as shown in Figure 3c. Specifically, when a large initial covariance matrix to account for arbitrary initial conditions is given, cubature gain, denoted as \mathbf{W} in Algorithm 1, becomes large. This leads to an adjustment of the phase estimate toward the measurement (i.e., the HR phase), which is independent of the initial conditions of the central clock state. This algorithmic procedure rapidly negates the undesired influence of initial conditions, which is not available in the previous methods solely relying on the convergence nature of a van der Pol limit cycle [26, 57]. Importantly, in the analysis of real data, our method more rapidly negated the influence of initial conditions (< 10 days) than the method based solely on the model prediction, as shown in Figures 7a, 7b, and 7e. This indicates the applicability of our method in real-life settings, where minimizing the effect of the initial conditions is desired.

In this study, a recently developed new extension of Kalman filtering named the level set Kalman filter [59] was used to integrate the model prediction with the physiological proxies extracted from wearable data. To the best of our knowledge, our work is the first attempt to use a Kalman filter to estimate the master clock phase in real-life settings from wearable data. It has been previously used to reduce the computational cost of performing the maximum likelihood estimation of physiological parameters of core body temperature rhythms [9]. Specifically, the standard discrete-time Kalman filter was exploited to efficiently compute the Cholesky factor of the inverse of the covariance matrix of maximum likelihood estimates. Considering this, our approach based on the Kalman filter for continuous-discrete systems sets the stage for utilizing wearable data to predict the human circadian phase.

Our filtering problem was tackled by using the recently proposed LSKF [59]. It tracks a Gaussian level set over time to solve the local linear approximation of the Fokker-Planck equation instead of calculating the moments of distribution as shown in Figure 2a. This novel approach to filtering problems can be applied to solve the chemical Langevin equation, a diffusion approximation of the chemical master equation describing stochastic dynamics of chemical systems [50]. It would be interesting in future work to compare its performance with existing methods such as the system size expansion [56] and moment closure approximations [19].

Our LSKF-based filtering approach also has broad applicability in biological studies. Specifically, it can estimate the experimentally unobservable (i.e., hidden) biochemical parameters [14, 32, 54]. For instance, the estimation problem of unobservable time-varying protein production rate \mathbf{m}_t^1 and degradation rate \mathbf{m}_t^2 can be formulated as a filtering problem with the model of the form

$$\begin{aligned} d\mathbf{m}_t &= \mathbf{v}(\mathbf{m}_t, t)dt + \sqrt{\mathbf{K}}dW_t \\ \dot{\mathbf{p}}_k &= \mathbf{m}_{t_k}^1 - \mathbf{m}_{t_k}^2 \mathbf{p}_k + \epsilon_k \end{aligned} \quad (41)$$

where $\mathbf{m}_t = [\mathbf{m}_t^1 \ \mathbf{m}_t^2]^T$ whose dynamics is described with a nonlinear drift function \mathbf{v} , \mathbf{p}_k and $\dot{\mathbf{p}}_k$ denote the protein abundance and its derivative, respectively, that can be measured with experimental techniques such as bioluminescence [43]. Note that \mathbf{v} is chosen depending on the protein of interest.

Our method can estimate the circadian phase with low uncertainty from wearables compared with the others as shown in Figures 6f and 7e. This benefit is preserved for a range of the parameter $\sigma_{\mathbf{K}}$ of the process noise matrix, as shown in Figure 7f. This demonstrates the capabilities of our method for tracking the circadian phase. In the analysis of the real-world data, we used the process noise matrix \mathbf{K} that was identified in the uncertainty analysis with *in-silico* data mimicking a typical human lifestyle in Figure 6. This strategy based on a typical case might not be suitable because there is accumulating evidence for a

large inter-and intraindividual variability in circadian variables [33]. Thus, a more systematic approach needs to be developed to tailor \mathbf{K} and the other model parameters to individual circadian physiology, which is an interesting avenue for future research.

Accurate estimation of circadian phase and its uncertainty enables personalized and real-time monitoring of progression of various diseases, including viral, bacterial, and neurodegenerative diseases [35, 36, 40, 42]. For instance, it has been recently shown that COVID-19 symptom onset correlates with an increased circadian phase uncertainty in [40]. Thus, the phase and its uncertainty accurately estimated by our method can be exploited for early disease diagnosis in real-world settings. Furthermore, accurate circadian phase estimation benefits sleep scoring based on wearable data. Specifically, it has been shown that the phase extracted only using the mathematical model can increase the accuracy of the sleep scoring machine-learning algorithm in [57]. Thus, more abundant and accurate information about the circadian phase is expected to enhance the accuracy of the existing wearable-based sleep scoring algorithms. This promising clinical applicability demonstrates that our filtering approach may provide an important advance in precision medicine in real-life conditions.

References

- [1] I. ARASARATNAM AND S. HAYKIN, *Cubature kalman filters*, IEEE Transactions on automatic control, 54 (2009), pp. 1254–1269.
- [2] I. ARASARATNAM, S. HAYKIN, AND T. R. HURD, *Cubature kalman filtering for continuous-discrete systems: theory and simulations*, IEEE Transactions on Signal Processing, 58 (2010), pp. 4977–4993.
- [3] L. BECKER AND N. ROHLEDER, *Time course of the physiological stress response to an acute stressor and its associations with the primacy and recency effect of the serial position curve*, PLoS One, 14 (2019), p. e0213883.
- [4] C. BOWMAN, Y. HUANG, O. J. WALCH, Y. FANG, E. FRANK, J. TYLER, C. MAYER, C. STOCKBRIDGE, C. GOLDSTEIN, S. SEN, ET AL., *A method for characterizing daily physiology from widely used wearables*, Cell reports methods, 1 (2021), p. 100058.
- [5] P. C. BRESSLOFF, *Stochastic processes in cell biology*, vol. 41, Springer, 2014.
- [6] E. N. BROWN, Y. CHOE, H. LUITHARDT, AND C. A. CZEISLER, *A statistical model of the human core-temperature circadian rhythm*, American Journal of Physiology-Endocrinology and Metabolism, 279 (2000), pp. E669–E683.
- [7] E. N. BROWN AND C. A. CZEISLER, *The statistical analysis of circadian phase and amplitude in constant-routine core-temperature data*, Journal of Biological Rhythms, 7 (1992), pp. 177–202.
- [8] E. N. BROWN AND H. LUITHARDT, *Statistical model building and model criticism for human circadian data*, Journal of Biological Rhythms, 14 (1999), pp. 609–616.
- [9] E. N. BROWN AND C. H. SCHMID, *Application of the kalman filter to computational problems in statistics*, in Methods in enzymology, vol. 240, Elsevier, 1994, pp. 171–181.
- [10] M. BUCKERT, C. SCHWIEREN, B. M. KUDIELKA, AND C. J. FIEBACH, *Acute stress affects risk taking but not ambiguity aversion*, Frontiers in neuroscience, 8 (2014), p. 82.
- [11] C. DIBNER, U. SCHIBLER, AND U. ALBRECHT, *The mammalian circadian timing system: organization and coordination of central and peripheral clocks*, Annual review of physiology, 72 (2010), pp. 517–549.
- [12] D.-J. DIJK, J. F. DUFFY, E. J. SILVA, T. L. SHANAHAN, D. B. BOIVIN, AND C. A. CZEISLER, *Amplitude reduction and phase shifts of melatonin, cortisol and other circadian rhythms after a gradual advance of sleep and light exposure in humans*, PloS one, 7 (2012), p. e30037.
- [13] D. B. FORGER, *The modeling of circadian oscillators*. B.S. Thesis. Harvard University, Cambridge, MA, 1999.

-
- [14] D. B. FORGER, *Biological clocks, rhythms, and oscillations: the theory of biological timekeeping*, (2017).
- [15] D. B. FORGER, M. E. JEWETT, AND R. E. KRONAUER, *A simpler model of the human circadian pacemaker*, *Journal of biological rhythms*, 14 (1999), pp. 533–538.
- [16] D. B. FORGER AND R. E. KRONAUER, *Reconciling mathematical models of biological clocks by averaging on approximate manifolds*, *SIAM Journal on Applied Mathematics*, 62 (2002), pp. 1281–1296.
- [17] D. B. FORGER AND D. PAYDARFAR, *Starting, stopping, and resetting biological oscillators: in search of optimum perturbations*, *Journal of theoretical biology*, 230 (2004), pp. 521–532.
- [18] D. B. FORGER AND C. S. PESKIN, *A detailed predictive model of the mammalian circadian clock*, *Proceedings of the National Academy of Sciences*, 100 (2003), pp. 14806–14811.
- [19] C. S. GILLESPIE, *Moment-closure approximations for mass-action models*, *IET systems biology*, 3 (2009), pp. 52–58.
- [20] J. GOODMAN AND J. WEARE, *Ensemble samplers with affine invariance*, *Communications in applied mathematics and computational science*, 5 (2010), pp. 65–80.
- [21] K. M. HANNAY, V. BOOTH, AND D. B. FORGER, *Macroscopic models for human circadian rhythms*, *Journal of Biological Rhythms*, 34 (2019), pp. 658–671.
- [22] K. M. HANNAY, D. B. FORGER, AND V. BOOTH, *Macroscopic models for networks of coupled biological oscillators*, *Science advances*, 4 (2018), p. e1701047.
- [23] H. C. HELLER, S. GLOTZBACH, D. GRAHN, AND C. RADEKE, *Sleep-dependent changes in the thermoregulatory system*, in *Clinical physiology of sleep*, Springer, 1988, pp. 145–158.
- [24] J. HONG, S. J. CHOI, S. H. PARK, H. HONG, V. BOOTH, E. Y. JOO, AND J. K. KIM, *Personalized sleep-wake patterns aligned with circadian rhythm relieve daytime sleepiness*, *IScience*, 24 (2021), p. 103129.
- [25] S. HONMA, *The mammalian circadian system: a hierarchical multi-oscillator structure for generating circadian rhythm*, *The Journal of Physiological Sciences*, 68 (2018), pp. 207–219.
- [26] Y. HUANG, C. MAYER, P. CHENG, A. SIDDULA, H. J. BURGESS, C. DRAKE, C. GOLDSTEIN, O. WALCH, AND D. B. FORGER, *Predicting circadian phase across populations: a comparison of mathematical models and wearable devices*, *Sleep*, 44 (2021), p. zsab126.
- [27] P. INDIC AND E. N. BROWN, *Characterizing the amplitude dynamics of the human core-temperature circadian rhythm using a stochastic-dynamic model*, *Journal of theoretical biology*, 239 (2006), pp. 499–506.
- [28] P. INDIC, D. B. FORGER, M. A. S. HILAIRE, D. A. DEAN, E. N. BROWN, R. E. KRONAUER, E. B. KLERMAN, AND M. E. JEWETT, *Comparison of amplitude recovery dynamics of two limit cycle oscillator models of the human circadian pacemaker*, *Chronobiology international*, 22 (2005), pp. 613–629.
- [29] M. E. JEWETT, D. B. FORGER, AND R. E. KRONAUER, *Revised limit cycle oscillator model of human circadian pacemaker*, *Journal of biological rhythms*, 14 (1999), pp. 493–500.
- [30] R. E. KALMAN AND R. S. BUCY, *New results in linear filtering and prediction theory*, (1961).
- [31] D. W. KIM, C. CHANG, X. CHEN, A. C. DORAN, F. GAUDREAU, T. WAGER, G. J. DEMARCO, AND J. K. KIM, *Systems approach reveals photosensitivity and per 2 level as determinants of clock-modulator efficacy*, *Molecular systems biology*, 15 (2019), p. e8838.
- [32] D. W. KIM, H. HONG, AND J. K. KIM, *Systematic inference identifies a major source of heterogeneity in cell signaling dynamics: The rate-limiting step number*, *Science advances*, 8 (2022), p. eabl4598.
- [33] D. W. KIM, E. ZAVALA, AND J. K. KIM, *Wearable technology and systems modeling for personalized chronotherapy*, *Current Opinion in Systems Biology*, 21 (2020), pp. 9–15.

- [34] R. KRONAUER, *A quantitative model for the effects of light on the amplitude and phase of the deep circadian pacemaker, based on human data*, *Sleep*, 90 (1990), pp. 306–309.
- [35] P. LI, L. YU, A. S. LIM, A. S. BUCHMAN, F. A. SCHEER, S. A. SHEA, J. A. SCHNEIDER, D. A. BENNETT, AND K. HU, *Fractal regulation and incident alzheimer’s disease in elderly individuals*, *Alzheimer’s & Dementia*, 14 (2018), pp. 1114–1125.
- [36] X. LI, J. DUNN, D. SALINS, G. ZHOU, W. ZHOU, S. M. SCHÜSSLER-FIORENZA ROSE, D. PERELMAN, E. COLBERT, R. RUNGE, S. REGO, ET AL., *Digital health: tracking physiomes and activity using wearable biosensors reveals useful health-related information*, *PLoS biology*, 15 (2017), p. e2001402.
- [37] W. R. LOVALLO, N. H. FARAG, A. S. VINCENT, T. L. THOMAS, AND M. F. WILSON, *Cortisol responses to mental stress, exercise, and meals following caffeine intake in men and women*, *Pharmacology Biochemistry and Behavior*, 83 (2006), pp. 441–447.
- [38] A. MARTINEZ-NICOLAS, J. A. MADRID, F. GARCÍA, M. CAMPOS, M. T. MORENO-CASBAS, P. F. ALMAIDA-PAGÁN, A. LUCAS-SÁNCHEZ, AND M. A. ROL, *Circadian monitoring as an aging predictor*, *Scientific reports*, 8 (2018), pp. 1–11.
- [39] M. M. MASSIN, K. MAEYNS, N. WITHOFS, F. RAVET, AND P. GÉRARD, *Circadian rhythm of heart rate and heart rate variability*, *Archives of disease in childhood*, 83 (2000), pp. 179–182.
- [40] C. MAYER, J. TYLER, Y. FANG, C. FLORA, E. FRANK, M. TEWARI, S. W. CHOI, S. SEN, AND D. B. FORGER, *Consumer-grade wearables identify changes in multiple physiological systems during covid-19 disease progression*, *Cell Reports Medicine*, 3 (2022), p. 100601.
- [41] C. MOTT, G. DUMONT, D. B. BOIVIN, AND D. MOLLICONE, *Model-based human circadian phase estimation using a particle filter*, *IEEE Transactions on Biomedical Engineering*, 58 (2011), pp. 1325–1336.
- [42] A. NATARAJAN, H.-W. SU, AND C. HENEGHAN, *Assessment of physiological signs associated with covid-19 measured using wearable devices*, *NPJ digital medicine*, 3 (2020), pp. 1–8.
- [43] M. A. PALEY AND J. A. PRESCHER, *Bioluminescence: a versatile technique for imaging cellular and molecular features*, *MedChemComm*, 5 (2014), pp. 255–267.
- [44] S. PANDA, *The arrival of circadian medicine*, *Nature Reviews Endocrinology*, 15 (2019), pp. 67–69.
- [45] M. D. RUBEN, D. F. SMITH, G. A. FITZGERALD, AND J. B. HOGENESCH, *Dosing time matters*, *Science*, 365 (2019), pp. 547–549.
- [46] J. A. SANDERS, F. VERHULST, AND J. MURDOCK, *Averaging methods in nonlinear dynamical systems*, vol. 59, Springer, 2007.
- [47] S. SÄRKKÄ, *Bayesian filtering and smoothing*, no. 3, Cambridge university press, 2013.
- [48] S. SÄRKKÄ AND A. SOLIN, *On continuous-discrete cubature kalman filtering*, *IFAC Proceedings Volumes*, 45 (2012), pp. 1221–1226.
- [49] F. A. SCHEER, K. HU, H. EVONIUK, E. E. KELLY, A. MALHOTRA, M. F. HILTON, AND S. A. SHEA, *Impact of the human circadian system, exercise, and their interaction on cardiovascular function*, *Proceedings of the National Academy of Sciences*, 107 (2010), pp. 20541–20546.
- [50] D. SCHNOERR, G. SANGUINETTI, AND R. GRIMA, *Approximation and inference methods for stochastic biochemical kinetics—a tutorial review*, *Journal of Physics A: Mathematical and Theoretical*, 50 (2017), p. 093001.
- [51] J. A. SETHIAN, *Curvature and the evolution of fronts*, *Communications in Mathematical Physics*, 101 (1985), pp. 487–499.

-
- [52] J. E. STONE, X. L. AUBERT, H. MAASS, A. J. PHILLIPS, M. MAGEE, M. E. HOWARD, S. W. LOCKLEY, S. M. RAJARATNAM, AND T. L. SLETTEN, *Application of a limit-cycle oscillator model for prediction of circadian phase in rotating night shift workers*, Scientific reports, 9 (2019), pp. 1–12.
- [53] G. SULLI, E. N. MANOOGIAN, P. R. TAUB, AND S. PANDA, *Training the circadian clock, clocking the drugs, and drugging the clock to prevent, manage, and treat chronic diseases*, Trends in pharmacological sciences, 39 (2018), pp. 812–827.
- [54] X. SUN, L. JIN, AND M. XIONG, *Extended kalman filter for estimation of parameters in nonlinear state-space models of biochemical networks*, PloS one, 3 (2008), p. e3758.
- [55] J. S. TAKAHASHI, *Transcriptional architecture of the mammalian circadian clock*, Nature Reviews Genetics, 18 (2017), pp. 164–179.
- [56] N. G. VAN KAMPEN, *Stochastic processes in physics and chemistry*, vol. 1, Elsevier, 1992.
- [57] O. WALCH, Y. HUANG, D. FORGER, AND C. GOLDSTEIN, *Sleep stage prediction with raw acceleration and photoplethysmography heart rate data derived from a consumer wearable device*, Sleep, 42 (2019), p. zsz180.
- [58] O. J. WALCH, A. COCHRAN, AND D. B. FORGER, *A global quantification of “normal” sleep schedules using smartphone data*, Science advances, 2 (2016), p. e1501705.
- [59] N. WANG AND D. FORGER, *The level set kalman filter for state estimation of continuous-discrete systems*, IEEE Transactions on Signal Processing, (2021).
- [60] A. WICHNIAK, K. S. JANKOWSKI, M. SKALSKI, K. SKWARŁO-SOŃTA, J. B. ZAWILSKA, M. ŻAROWSKI, E. PORADOWSKA, AND W. JERNAJCZYK, *Treatment guidelines for circadian rhythm sleep-wake disorders of the polish sleep research society and the section of biological psychiatry of the polish psychiatric association. part i. physiology, assessment and therapeutic methods*, Psychiatr Pol, 51 (2017), pp. 793–814.
- [61] T. WOELDERS, D. G. BEERSMA, M. C. GORDIJN, R. A. HUT, AND E. J. WAMS, *Daily light exposure patterns reveal phase and period of the human circadian clock*, Journal of biological rhythms, 32 (2017), pp. 274–286.
- [62] R. ZHANG, N. F. LAHENS, H. I. BALLANCE, M. E. HUGHES, AND J. B. HOGENESCH, *A circadian gene expression atlas in mammals: implications for biology and medicine*, Proceedings of the National Academy of Sciences, 111 (2014), pp. 16219–16224.
- [63] L. ZHU AND P. C. ZEE, *Circadian rhythm sleep disorders*, Neurologic clinics, 30 (2012), pp. 1167–1191.
- [64] L. A. ZUURBIER, A. I. LUIK, A. HOFMAN, O. H. FRANCO, E. J. VAN SOMEREN, AND H. TIEMEIER, *Fragmentation and stability of circadian activity rhythms predict mortality: the rotterdam study*, American journal of epidemiology, 181 (2015), pp. 54–63.